

$X^1\Sigma^+$ and $a^3\Sigma^+$ states of the atom pair K+Cs studied by Fourier-transform spectroscopy

R. Ferber, I. Klinkare, O. Nikolayeva, and M. Tamanis

Laser Center, University of Latvia, Rainis Boulevard 19, LV-1586 Riga, Latvia

H. Knöckel and E. Tiemann

Institute of Quantum Optics, Leibniz University Hannover, Welfengarten 1, 30167 Hannover, Germany

A. Pashov

Department of Physics, Sofia University, 5 J. Bourchier Boulevard, 1164 Sofia, Bulgaria

(Received 31 July 2009; published 1 December 2009)

A comprehensive study of the $X^1\Sigma^+$ and $a^3\Sigma^+$ electronic states of the K and Cs atom pair is presented. Abundant spectroscopic data include 1937 transitions to the $a^3\Sigma^+$ state and 13 724 transitions to the $X^1\Sigma^+$ state for $^{39}\text{K } ^{133}\text{Cs}$ which were obtained by Fourier-transform spectroscopy. From these data potential energy curves were constructed simultaneously for both states $X^1\Sigma^+$ and $a^3\Sigma^+$ which are coupled by the hyperfine interaction. This allows us to accurately model the potential close to $\text{K}(4s)+\text{Cs}(6s)$ atom-pair asymptote which is required to simulate cold collision processes. Dissociation energies of the $X^1\Sigma^+$ state as $D_e^X=4069.208(40) \text{ cm}^{-1}$ and of the $a^3\Sigma^+$ state as $D_e^a=267.141(20) \text{ cm}^{-1}$ were determined. Scattering lengths are predicted for different KCs isotopologs and Feshbach resonances were calculated for magnetic fields up to 1000 G.

DOI: [10.1103/PhysRevA.80.062501](https://doi.org/10.1103/PhysRevA.80.062501)

PACS number(s): 34.50.Cx, 33.20.Kf, 33.20.Vq, 31.50.Bc

I. INTRODUCTION

Quantum gases of polar diatomic alkali-metal molecules have attracted researchers due to their ability to interact at large distances by the dipole-dipole force (see [1] for a review). These properties might be observable when polar molecules are produced at ultracold temperatures. Heteronuclear alkali-metal diatomic molecules are also proposed for using them as qubits in a quantum processor [2] and in high precision measurements of fundamental constants [3–5], as well as for development of coherently controlled ultracold chemical reactions [6]. Such ultracold species are most often produced from ultracold atoms in mixed atomic traps by either photoassociation or magnetic field induced Feshbach resonances. With diatomic molecules containing either a K or Cs atom successful experiments were done in this field on KRb [7–11], LiCs [12,13], NaCs [14,15], and RbCs [16,17] but nothing on KCs. It seems useful to involve KCs into the search of the prospective objects since exploring many systems provides more flexibility for experimenters and has the potential for finding a system with favorable properties.

To plan and perform such experiments, there is strong need of accurate knowledge of the ground state potential energy curve (PEC) of the diatomic species close to their asymptotic limit of the respective atomic pairs. Substantial progress in examining the ground state asymptotes of pairs of different alkali-metal atoms was achieved by applying high resolution Fourier-transform spectroscopy of laser-induced fluorescence (LIF) and evaluating the data by coupled channel treatment which accounted for the hyperfine mixing of the $X^1\Sigma^+$ and $a^3\Sigma^+$ states (see [18] for NaRb, [19] for NaCs, [20] for LiCs, and [21] for KRb). The most comprehensive study was carried out on the KRb molecule at the $\text{K}(4s)+\text{Rb}(5s)$ atomic asymptote in which abundant

spectroscopic data for $^{39}\text{K } ^{85}\text{Rb}$ and $^{39}\text{K } ^{87}\text{Rb}$ have been collected covering a wide range of vibrational and rotational energy levels of the $a^3\Sigma^+$ state with outer turning points up to 14.6 Å. Inclusion of the observed Feshbach resonances [10] into the data fitting routine yielded a complete physical model allowing us to predict scattering lengths and Feshbach resonances extended to other KRB isotopologs. The accuracy of the dissociation energy of the singlet state obtained in [21] appeared competing to its counterpart obtained in [8] from a photoassociation-depletion process used to determine binding energies of loosely bound levels. The potential of $\text{K}(4s)$ and $\text{Rb}(5s)$ pairs given in [21] was used by Ni *et al.* [7] to calculate the term values needed for a successful experiment on efficient transformation of the respective ultracold atoms into the triplet ground state $a^3\Sigma^+$ with vibrational quantum number $v''=0$ as well as into the absolute ground state $X^1\Sigma^+(v''=0, J''=0)$ of the KRb molecule, J'' being the rotational quantum number. For the LiCs molecule, the empirical singlet and triplet state potentials in [20] facilitated successful formation of ultracold LiCs in its absolute rovibrational ground state as achieved in [13].

Though KRb is probably the heteronuclear species mostly discussed for applications of ultracold matter for fundamental studies such as quantum computation or modeling of condensed matter physics, KCs might offer advantage because of a very rich spectrum of Feshbach resonances. This is related to the high nuclear spin of Cs and the large ratio between the K and the Cs nuclear hyperfine coupling constants. Additionally, KCs is heavier and has a larger electric dipole moment than KRb [22], which both help us to manipulate the quantum states by electric fields for studies of quantum phase transitions in dipolar gasses or for quantum information developments. Thus, there is strong motivation for studying the $\text{K}(4s)$ and $\text{Cs}(6s)$ atomic asymptote and the coupling of the $X^1\Sigma^+$ and $a^3\Sigma^+$ ground states of the KCs

molecule. The KCs molecule is spectroscopically known only recently from our previous work [23] in which 7226 term values for the ground $X^1\Sigma^+$ state covering a range $v''=0-97$ and $J''=12-209$ yielded an empirical pointwise PEC through the inverted perturbation approach (IPA) routine [29]. The IPA PEC covers more than 99.5% of the well depth of the $X^1\Sigma^+$ state and reproduces the vast majority of the more than 10 000 obtained spectral lines with an accuracy of about 0.003 cm^{-1} . It should be noted, however, that for the highest observed vibrational levels from $v''=91-97$ the accuracy of the PEC was not as good due to mixing between $X^1\Sigma^+$ and $a^3\Sigma^+$ states, which was ignored in the single potential approach. As a result, a considerably increased scatter of deviations has been obtained for $v''>90$, with maximum deviation for $v''=94$. As demonstrated in [18–21], application of coupled channel treatment accounting for hyperfine mixing between $X^1\Sigma^+$ and $a^3\Sigma^+$ states is crucial for improving the PEC for higher vibrational levels and the accuracy of the dissociation energy value and for simulating cold collisions. To accomplish this task, it is necessary to have a good coverage of accurate data on the term values of the triplet ground state $a^3\Sigma^+$. Though this state has been observed and few preliminary molecular constants have been presented in [23], these data are far from being sufficient for performing the coupled channel fit.

In the course of the present study we, first, found proper laser excitation frequencies which give rise to fluorescence to $a^3\Sigma^+$ and then applied high resolution Fourier-transform spectroscopy to collect abundant amount of data for the $a^3\Sigma^+$ state of the KCs molecules, allowing us to construct simultaneously experiment based PECs for both states $X^1\Sigma^+$ and $a^3\Sigma^+$ coupled by the hyperfine interaction. This will allow us to accurately derive the PECs close to $K(4s)+Cs(6s)$ atom-pair asymptote which is required to model cold collision processes.

To widen considerably the data range of the $a^3\Sigma^+$ state it was necessary to record LIF spectra connected to the large variety of the vibrational and rotational levels of the $a^3\Sigma^+$ state. For this purpose LIF from the $B(1)^1\Pi$ state perturbed by the $c^3\Sigma^+$ state was used and additionally LIF from the $(4)^1\Sigma^+$ state (see Fig. 1). The selection of excitation frequency ranges was based on reliable *ab initio* calculations for KCs available from [24–26]. It should be noted that the heteronuclear alkali-metal dimers in their $a^3\Sigma^+$ states are much more favorable for spectroscopic studies than homonuclear ones since one-color (one-step) LIF excitation windows can be found whereas for homonuclear dimers more sophisticated excitation schemes are to be applied because of the $u \leftrightarrow g$ parity selection rule (see, for instance, [27] for K_2 and [28] for Cs_2).

The present paper is structured as follows. After describing the experimental approach in Sec. II, the analysis of the obtained spectra is presented in Sec. III. The construction of the empirical potential energy curves are reported in Sec. IV, while Sec. V deals with their application to modeling cold collisions, followed by a concluding discussion in Sec. VI.

II. EXPERIMENT

The experimental setup was the same as for the studies of the ground state of KCs [23]. Briefly, the KCs molecules

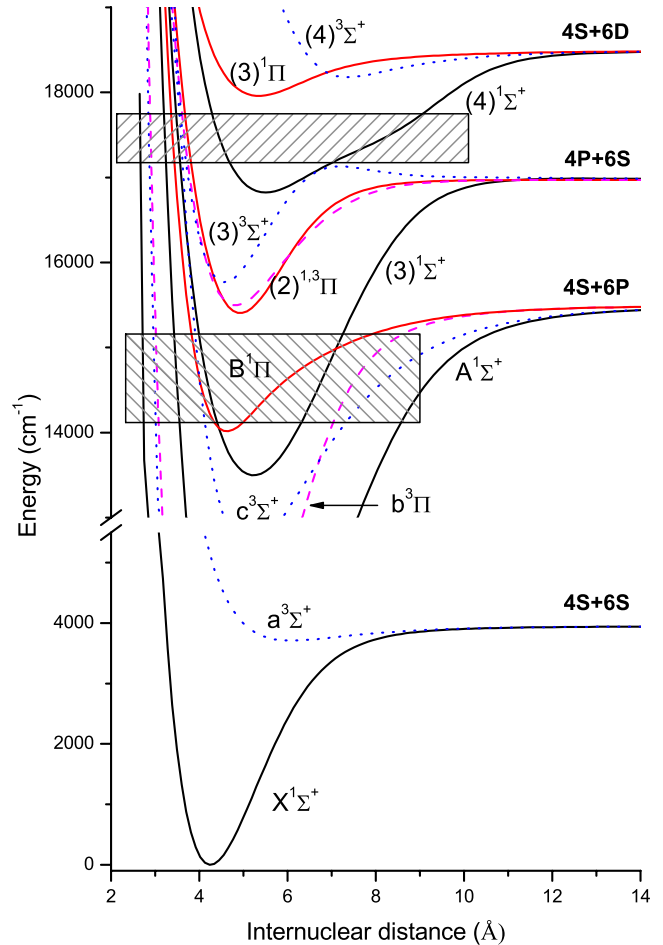


FIG. 1. (Color online) Scheme of potential energy curves for selected low lying singlet (solid lines) and triplet states (dashed lines) of KCs molecule taken from Ref. [24]. Hatched blocks indicate areas of excited state energies reached by Rhodamine 6 G dye laser and diode laser excitation.

were produced in a linear heat pipe at temperatures around $280\text{ }^\circ\text{C}$. LIF was collected by a pierced mirror in the direction opposite to the laser beam propagation through the heat pipe and recorded by a Bruker IFS 125 HR Fourier-transform spectrometer with typical resolution of 0.03 cm^{-1} . The uncertainty of the line positions is estimated to be 0.1 of the resolution. For lines with signal-to-noise ratio less than 3 the uncertainty is gradually increased, reaching 0.01 cm^{-1} for signal-to-noise ratio of about 2.

The general sequence of the measurement process was the following. The laser frequency was tuned until the LIF signal monitored in the “preview mode” of the spectrometer (operated at strongly reduced resolution) gets its maximal value at the frequency range which is expected for the transitions to the $a^3\Sigma^+$ state and then fixed while recording the fluorescence with high resolution. We used various laser sources for observing transitions to the $a^3\Sigma^+$ state. First, for the range around $17\,250\text{ cm}^{-1}$, we applied a Rhodamine 6 G dye laser (Coherent 699-21) for excitation of the state $(4)^1\Sigma^+$ which, as was reported in [23], gives LIF to the $a^3\Sigma^+$ state along with strong fluorescence to the ground state $X^1\Sigma^+$. These frequencies appeared to cause stronger LIF to the $a^3\Sigma^+$ state

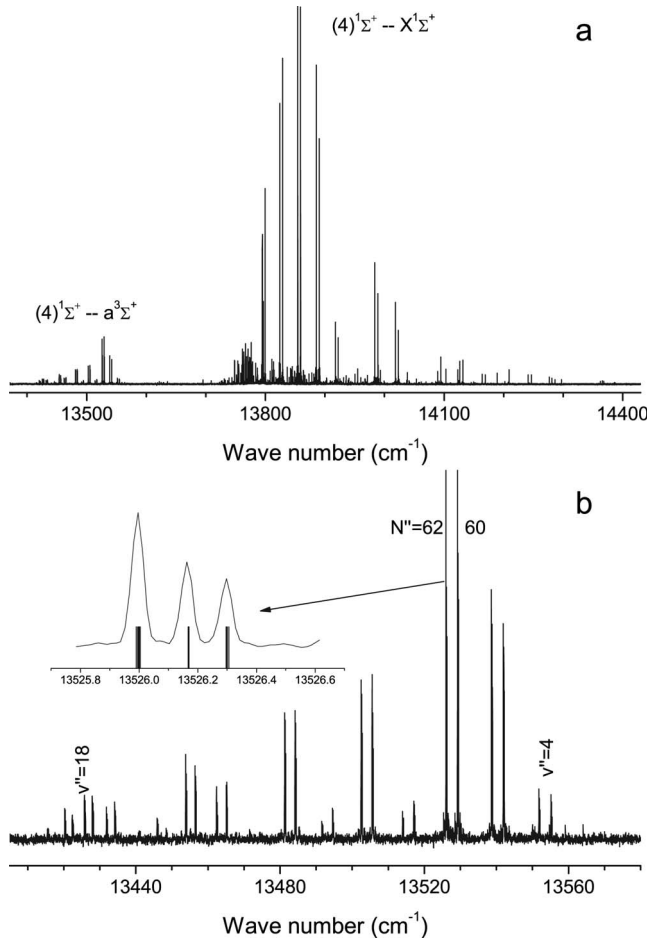


FIG. 2. (a) Fluorescence progressions to $a^3\Sigma^+$ and $X^1\Sigma^+$ states originating from the perturbed $(4)^1\Sigma^+$ state levels excited by a Rhodamine 6 G dye laser at $17\,266.022\text{ cm}^{-1}$. The high frequency part of the spectrum to $X^1\Sigma^+$ is cut by a long-pass edge filter. (b) Details of the triplet progression $(4)^1\Sigma^+ \rightarrow a^3\Sigma^+$ covering $v'' = 4-19$. The inset in (b) represents the hyperfine splitting of the rotational level with $N''=62$ in $^{39}\text{K } ^{133}\text{Cs}$; vertical lines mark the calculated positions of hyperfine components. N'' is the rotational quantum number for the $a^3\Sigma^+$ state which is close to Hund's coupling case b .

than the frequencies of about $16\,870\text{ cm}^{-1}$ used in [23]. The laser power at the entrance window of the heat pipe was about 150 mW. When the laser was fixed at selected frequencies ranging from $17\,211$ to $17\,298\text{ cm}^{-1}$, we recorded a number of additional spectra containing $(4)^1\Sigma^+ \rightarrow a^3\Sigma^+$ transitions. For detection we used a photomultiplier (Hamamatsu R928). Figure 2(a) presents a spectrum containing a part of the $(4)^1\Sigma^+ \rightarrow X^1\Sigma^+$ LIF progression, as well as one of the longest (stretching from $v''=4$ to $v''=19$) LIF progressions observed for $(4)^1\Sigma^+ \rightarrow a^3\Sigma^+$ with dye laser excitation; the spectrum is given in more detail in Fig. 2(b). The resolved hyperfine structure (HFS) shown in the inset of Fig. 2(b) clearly reveals the triplet nature of the lower state. Only a fragment of $(4)^1\Sigma^+ \rightarrow X^1\Sigma^+$ LIF can be seen in Fig. 2(a) because of a long-pass edge filter which cuts off light with frequencies higher than approximately $14\,200\text{ cm}^{-1}$.

The analysis of the progressions to the triplet state revealed that the $(4)^1\Sigma^+ \rightarrow a^3\Sigma^+$ transitions observed so far

did not include vibrational levels of the $a^3\Sigma^+$ state higher than $v''=21$. Looking for possibilities of enlarging the data field for the $a^3\Sigma^+$ state and remembering that in our previous studies of the $a^3\Sigma^+$ state in NaRb [18], NaCs [19], and KRb [21] molecules the $B(1)^1\Pi$ state was very useful for an access to the triplet manifold due to numerous local perturbations by the neighboring triplet states $c^3\Sigma^+$ and $b^3\Pi$ (see Fig. 1), we concentrated our further efforts on searching for appropriate excitations of $(B^1\Pi \sim c^3\Sigma^+ \sim b^3\Pi) \rightarrow a^3\Sigma^+$ LIF which for simplicity is denoted as $B^1\Pi \rightarrow a^3\Sigma^+$. From the PEC scheme in Fig. 1, one can expect that $B^1\Pi \leftarrow X^1\Sigma^+$ transitions could be excited with laser frequencies within the range of $13\,500-14\,600\text{ cm}^{-1}$. We decided to exploit diode lasers as excitation sources, similarly to the approach in [23]. We started with a 685 nm laser diode built in a homemade external cavity resonator and searched for triplet fluorescence from highly excited $B^1\Pi$ vibrational levels. The optical power from this diode was about 20 mW at the entrance window of the heat pipe, and a silicon (Si) diode was used as a detector. At excitation frequencies from $14\,600$ to about $14\,500\text{ cm}^{-1}$ rather strong LIF of K_2 was observed, sometimes with very weak admixture of LIF of KCs. The intensity of the KCs $B^1\Pi \rightarrow X^1\Sigma^+$ fluorescence increased by moving to lower excitation frequencies; however, the $B^1\Pi \rightarrow a^3\Sigma^+$ transitions remained weak and hardly distinguishable from the background in the preview mode.

Looking for stronger triplet transitions, we continued with lower excitation frequencies by applying a 705 nm laser diode (Optnext, 50 mW). Though the optical power of this diode at the entrance window of the heat pipe was also about 20 mW, the LIF signals containing both $B^1\Pi \rightarrow X^1\Sigma^+$ and $B^1\Pi \rightarrow a^3\Sigma^+$ progressions were stronger than with 685 nm laser diode excitation. In order to get an idea of an optimal excitation frequency for observation of triplet transitions, we recorded spectra at laser excitation frequencies in the range from $14\,320$ to $14\,070\text{ cm}^{-1}$. After analyzing these spectra a number of favorable laser frequencies were selected for repeated measurements. To improve the signal-to-noise ratio, especially for progressions including high vibrational levels of the $a^3\Sigma^+$ state, we applied the following steps: (i) we used long pass filters to cut strong scattered laser light as well as most of the strong $B^1\Pi \rightarrow X^1\Sigma^+$ LIF spectrum; (ii) in some cases we replaced the Si diode detector by InGaAs diode which appeared more sensitive in the spectral range below $10\,700\text{ cm}^{-1}$; and (iii) we increased the acquisition time in some cases up to 3 h. Figure 3(a) gives an example of the spectrum recorded with the InGaAs detector at the excitation frequency of $14\,304.309\text{ cm}^{-1}$. Here the strong $B^1\Pi \rightarrow X^1\Sigma^+$ progression is dramatically suppressed both by spectral sensitivity of the detector and by the long pass filter, thus only the very end of the $B \rightarrow X$ progressions is seen. Six $B^1\Pi \rightarrow a^3\Sigma^+$ LIF progressions have been assigned in this spectrum between $10\,250$ and $11\,000\text{ cm}^{-1}$; the strongest one is enlarged in Fig. 3(b).

III. ANALYSIS OF THE SPECTRA

In our previous work [23] we have observed and assigned in total 74 transitions to the $a^3\Sigma^+$ state covering $v''=1-11$

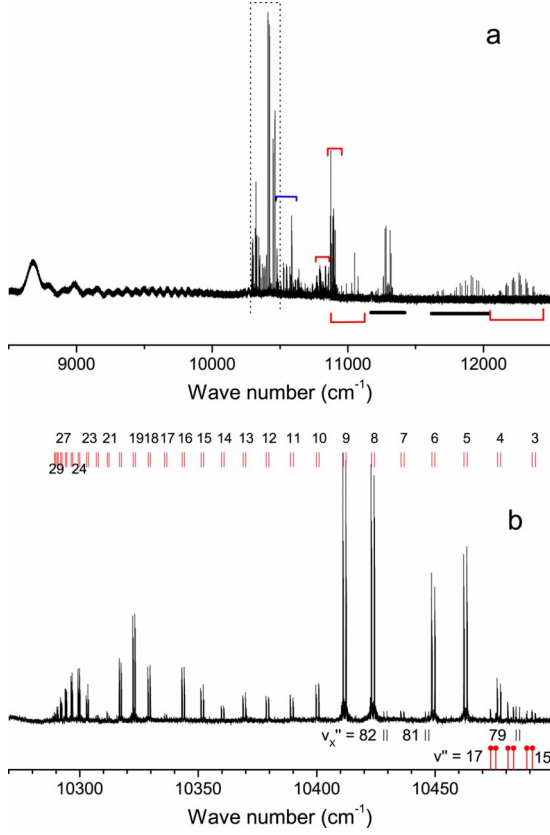


FIG. 3. (Color online) (a) Example of LIF spectra from the $B(1) {}^1\Pi$ state excited by a diode laser at $14\,304.309\text{ cm}^{-1}$. The high frequency part of the spectrum is cut off by a long-pass edge filter; the dashed box indicates the part which is zoomed in (b). The $B \rightarrow a$ progressions are marked above the spectrum. The $B \rightarrow X$ progressions are marked below the spectrum, by brackets the ones with corresponding progressions to the $a {}^3\Sigma^+$ state, and with solid segments in cases of no such progressions. (b) Part of the $(v', J' = 24) B {}^1\Pi \rightarrow a {}^3\Sigma^+$ progression covering v'' from 3 to 29 as marked at the top; transitions from the same v', J' to the $X {}^1\Sigma^+$ state with $v''_X = 79, 81$, and 82 are marked below. The vertical bars with filled circles indicate transitions to $a {}^3\Sigma^+$ state induced by Q excitation to the level $(v^*, J' = 28)$ of the $B {}^1\Pi$ state.

vibrational levels with rotational quantum number N'' from 41 to 143, which were used in the fit by the IPA method [29] for a preliminary pointwise PEC determination. This PEC was applied to assign the presently recorded transitions. Note that, due to hyperfine interactions in the $a {}^3\Sigma^+$ state, each fluorescence line to the triplet state is split into three components [see inset of Fig. 2(b)], which resembles the Cs hyperfine structure and contains unresolved multiplets due to the smaller hyperfine structure from K. In [23], as well as in the present study, the position of the middle component, being the closest to the hyperfine structure free position, was chosen for the line frequency estimate. The newly observed levels were added to the previous data field and the fitting was performed using step-by-step extended data fields providing an improved potential.

In such a way we gradually added higher $a {}^3\Sigma^+$ state v'' data to the fit, finally reaching $v'' = 29$. In some progressions transitions to $v'' = 0$ were found, thus confirming our previous

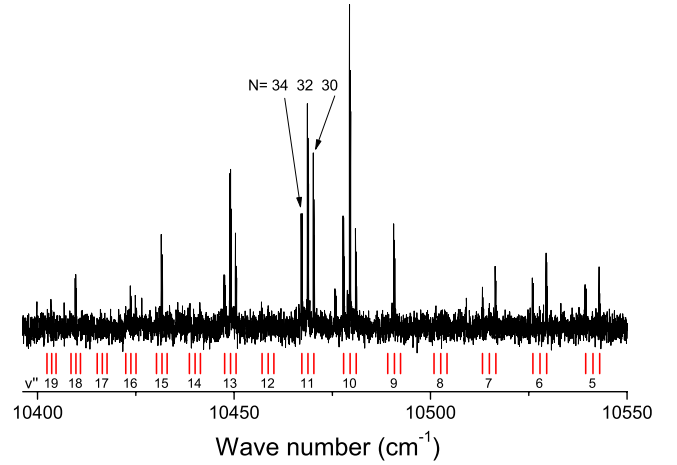


FIG. 4. (Color online) Fluorescence progression to the $a {}^3\Sigma^+$ state following Q excitation $(v^*, J' = 32) B {}^1\Pi \leftarrow (v'' = 2, J'' = 32) X {}^1\Sigma^+$, laser frequency $14\,241.243\text{ cm}^{-1}$.

vibrational numbering of the $a {}^3\Sigma^+$ state [23].

We observed in total 116 progressions (approximately 1930 lines) to the $a {}^3\Sigma^+$ state for ${}^{39}\text{K} {}^{133}\text{Cs}$ isotopolog, 48 of them applying excitation of the $(4) {}^1\Sigma^+$ state (by the dye laser with Rhodamin 6 G) and 68 applying excitation of the $B {}^1\Pi$ state (by the 705 nm laser diode). Only one fragmentary triplet progression for the isotopolog ${}^{41}\text{K} {}^{133}\text{Cs}$ has been recorded and identified. The energy regions of the $(4) {}^1\Sigma^+$ state and the $B {}^1\Pi$ state giving fluorescence to the $a {}^3\Sigma^+$ state are shown in Fig. 1 as hatched areas. Since for coupled channel calculations the exact energy difference between $a {}^3\Sigma^+$ and $X {}^1\Sigma^+$ levels is crucial, we analyzed all lines observed in the recorded spectra for the respective progressions to the singlet state $X {}^1\Sigma^+$ which originated from the same excited levels as the triplet progressions.

An analysis of the LIF spectrum from the $(4) {}^1\Sigma^+$ state presented in Fig. 2(a) reveals that the progression to the triplet state $a {}^3\Sigma^+$ ($v'' = 4-19$, $N'' = 62$ and 60) and the strongest progression to the singlet state $X {}^1\Sigma^+$ originate from a common upper state level $v^*, J' = 61$ with energy $E' = 17\,478.94\text{ cm}^{-1}$. The group of weaker lines around $13\,800\text{ cm}^{-1}$ belongs to another weak KCs progressions to the singlet state $X {}^1\Sigma^+$ but no corresponding transitions to the triplet state $a {}^3\Sigma^+$ were observed, most probably due to their weakness.

Figure 3(a) presents the $B \rightarrow a$ LIF spectrum which contains six progressions to the $a {}^3\Sigma^+$ state; the longest and strongest progression with $N'' = 23$ and 25 is presented in Fig. 3(b) and reaches $v'' = 29$.

Most of the observed $B \rightarrow a$ progressions consist of rotational doublets since they were obtained by excitation of the $B {}^1\Pi$ state in P or R type transitions with $J' = J'' - 1$ or $J' = J'' + 1$, respectively. However, some $B \rightarrow a$ progressions were observed under Q type excitation ($J' = J''$) of the $B {}^1\Pi$ state. Such progressions consist of rotational multiplets corresponding to $N'' = J' - 2$, $N'' = J'$, $N'' = J' + 2$ rotational quantum numbers of the $a {}^3\Sigma^+$ state and exhibit unusual intensity distribution among the rotational components for different vibrational levels v'' . An example of such behavior is pre-

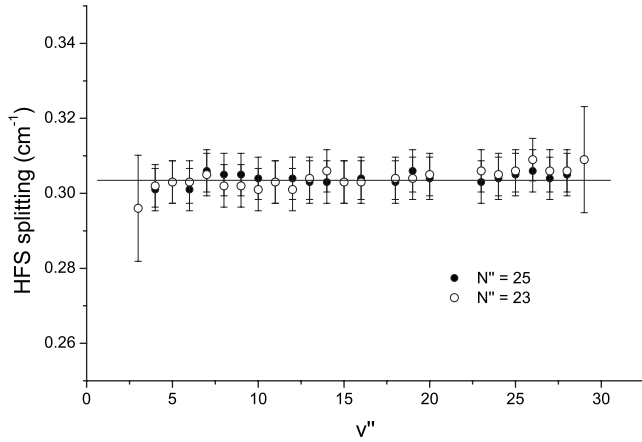


FIG. 5. Vibrational dependence of the overall hyperfine splitting of the $a\ ^3\Sigma^+$ state.

sented in Fig. 4 where the central component of the multiplet with $N''=32$ is the strongest for higher vibrational levels v'' but almost disappears for lower v'' from 5 to 7. It should be noted that a similar behavior was observed during the study of the $a\ ^3\Sigma^+$ state in the NaCs molecule [19] and it can be probably explained by the influence of the perturbed upper state, leading to a multicomponent wave function.

The HFS of the rotational lines consists of three groups of lines [see the inset in Fig. 2(b)], originating from the Fermi contact interaction in the case b_{FS} coupling scheme, yielding for deeply bound levels a coupling of the electron spin $S=1$ first with the nuclear spin $I=7/2$ of the Cs atom and then with the nuclear spin $I=3/2$ of the ^{39}K atom. The very small splitting due to the ^{39}K atom is not resolved in the present experiment. The observed HFS is well described by atomic HFS parameters of ^{133}Cs and ^{39}K . The central component of the HFS triplet is close to the center of gravity of the hyperfine structure and thus will serve as the frequency of a pure rovibrational transition for the first step in the analysis. Figure 5 shows the vibrational dependence of the overall hyperfine splitting for the progression in Fig. 3(b) with $N''=23$ and 25 and demonstrates its independence of v'' . However, con-

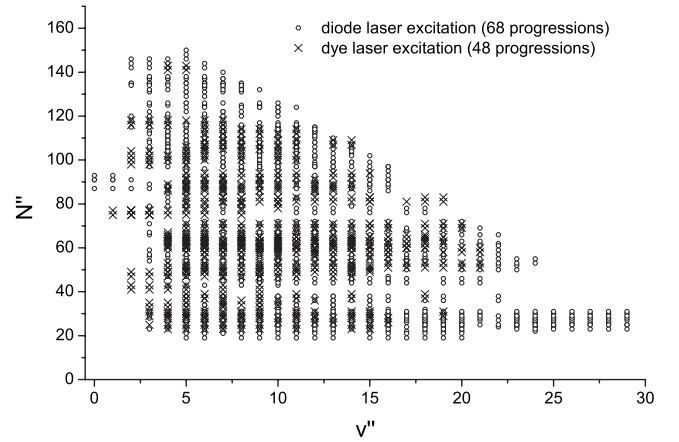


FIG. 7. Distribution over v'' and N'' of assigned LIF transitions to the $a\ ^3\Sigma^+$ state of KCs.

siderable deviations from such a typical HFS pattern are observed for the lines with particular v'' , N'' . This especially concerns the position of the middle HFS component [compare inset of Fig. 2(b)] which is not clearly recognizable for $v''=23$, $N''=57, 59$, as shown in Fig. 6. Such deviations will be discussed below by taking into account the hyperfine mixing of the weakly bound levels in states $X\ ^1\Sigma^+$ and $a\ ^3\Sigma^+$.

The final data field of the $a\ ^3\Sigma^+$ state is presented in Fig. 7; it contains 1231 levels with quantum numbers v'' from 0 to 29 and N'' from 19 to 150. The pointwise PEC derived in a single-channel approach (see Table I of the supplementary materials [30]) reproduces the $a\ ^3\Sigma^+$ state energies of the observed data field with a standard deviation of 0.0045 cm^{-1} when the data for $v''=23$ and 29 are excluded. The rotational levels of $v''=23$ are strongly mixed with the singlet state and therefore shifted from their “unperturbed” positions up to 0.1 cm^{-1} . The energies for $v''=29$ were not included in the fit as well since their assignment was doubtful due to moderate signal-to-noise ratio, and only a proper description of the long-range part by coupled channel calculations described below allowed us to include them into the final fit.

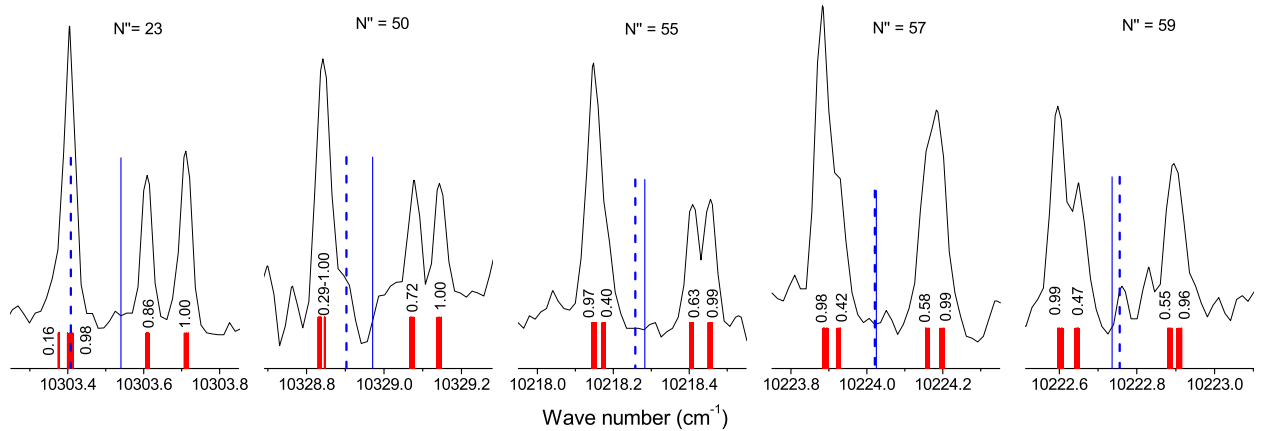


FIG. 6. (Color online) Observed transitions in $^{39}\text{K}\ ^{133}\text{Cs}$ to $v''=23$ in the neighborhood of $v''_X=94$ for different N'' as indicated in the figure. The calculated hyperfine pattern is given by short (red) sticks. The numbers close at sticks are the rounded expectation values of the total electron spin S for the group of the unresolved HFS components. The thin long (blue) sticks indicate the line positions as predicted by the Born-Oppenheimer PEC; solid lines denote transitions from the common upper level to the a state while dotted lines those to the X state.

TABLE I. Parameters of the analytic representation of the $X^1\Sigma^+$ state potential. The energy reference is the dissociation asymptote. Parameters with * are set for continuous extrapolation of the potential.

	$R < R_i = 3.185 \text{ \AA}$
A^*	$-0.496518516 \times 10^4 \text{ cm}^{-1}$
B^*	$0.645762476 \times 10^7 \text{ cm}^{-1} \text{ \AA}^{6.18977}$
	$R_i \leq R \leq R_o = 12.000 \text{ \AA}$
b	-0.39
R_m	4.28377150 \AA
a_0	$-4069.207927 \text{ cm}^{-1}$
a_1	$-0.432282543580656875 \text{ cm}^{-1}$
a_2	$0.142720993189201072 \times 10^5 \text{ cm}^{-1}$
a_3	$0.102549224826570935 \times 10^5 \text{ cm}^{-1}$
a_4	$-0.517006972284939548 \times 10^4 \text{ cm}^{-1}$
a_5	$-0.203527845348886112 \times 10^5 \text{ cm}^{-1}$
a_6	$-0.263658341774372020 \times 10^5 \text{ cm}^{-1}$
a_7	$-0.204605453877752552 \times 10^4 \text{ cm}^{-1}$
a_8	$0.319728702383779055 \times 10^5 \text{ cm}^{-1}$
a_9	$-0.477840898322073743 \times 10^6 \text{ cm}^{-1}$
a_{10}	$-0.721691441556341830 \times 10^6 \text{ cm}^{-1}$
a_{11}	$0.588637425284565240 \times 10^7 \text{ cm}^{-1}$
a_{12}	$0.612483418343720678 \times 10^7 \text{ cm}^{-1}$
a_{13}	$-0.448085869823485464 \times 10^8 \text{ cm}^{-1}$
a_{14}	$-0.309090839469884448 \times 10^8 \text{ cm}^{-1}$
a_{15}	$0.224019562226168901 \times 10^9 \text{ cm}^{-1}$
a_{16}	$0.112081516935981765 \times 10^9 \text{ cm}^{-1}$
a_{17}	$-0.715479987723696589 \times 10^9 \text{ cm}^{-1}$
a_{18}	$-0.272974605878372073 \times 10^9 \text{ cm}^{-1}$
a_{19}	$0.145087133254843497 \times 10^{10} \text{ cm}^{-1}$
a_{20}	$0.408938330109909654 \times 10^9 \text{ cm}^{-1}$
a_{21}	$-0.181717664310721707 \times 10^{10} \text{ cm}^{-1}$
a_{22}	$-0.338193881626500130 \times 10^9 \text{ cm}^{-1}$
a_{23}	$0.128707089212750936 \times 10^{10} \text{ cm}^{-1}$
a_{24}	$0.118285128401653573 \times 10^9 \text{ cm}^{-1}$
a_{25}	$-0.395477839057772458 \times 10^9 \text{ cm}^{-1}$
	$R > R_o$
$D_{\text{asymptote}} = U_\infty$	0.0 cm^{-1}
C_6	$0.2486300 \times 10^8 \text{ cm}^{-1} \text{ \AA}^6$
C_8	$0.8934100 \times 10^9 \text{ cm}^{-1} \text{ \AA}^8$
C_{10}	$0.3768824 \times 10^{11} \text{ cm}^{-1} \text{ \AA}^{10}$
A_{ex}	$0.3333495 \times 10^6 \text{ cm}^{-1} \text{ \AA}^{-\gamma}$
γ	4.88068
β	2.25698 \AA^{-1}
Derived constants	
Equilibrium distance	$R_e^X = 4.28381(5) \text{ \AA}$
Electronic term energy	$T_e^X = -4069.208(40) \text{ cm}^{-1}$

IV. EVALUATION OF THE SYSTEM $X^1\Sigma^+ - a^3\Sigma^+$

The rovibrational levels of the $a^3\Sigma^+$ state of the KCs were approximated by choosing the central line of the hyperfine multiplets and several observed transitions were excluded from the evaluation because of distorted hyperfine structure. Similarly, we reported in [23] about some rovibrational levels of state $X^1\Sigma^+$ which deviated strongly from their expected positions calculated from the best potential. All these effects have their origin in the hyperfine coupling of the system $X^1\Sigma^+ - a^3\Sigma^+$. Thus we will describe the joint evaluation of both states with their common atomic asymptote $K(4s) + \text{Cs}(6s)$. This procedure was already successfully applied in other cases, such as KRb [21]; therefore we will only put together the general formulas to define clearly the molecular parameters obtained by the fit of all spectroscopic data for both states $X^1\Sigma^+$ and $a^3\Sigma^+$.

The Hamiltonian for the system contains the kinetic energy of the nuclear motion, the potential energies of the states $X^1\Sigma^+$ and $a^3\Sigma^+$, and the hyperfine energy given as Fermi contact interaction for each atom (for details see, for example, Ref. [31]). The hyperfine parameters for each atom are taken from the compilation by Arimondo *et al.* [32], assuming insignificant variation of the hyperfine parameters with internuclear separation R due to chemical bond. This assumption is justified by observing the constancy of the hyperfine splitting as a function of vibrational state as given in Fig. 5. The potential energy functions for $X^1\Sigma^+$ and $a^3\Sigma^+$ are represented piecewise in analytic form for three different regions of R , the short range region with $R < R_i$, the deeply bound region with $R_i \leq R \leq R_o$, and the long-range region for $R > R_o$.

The analytic form of each potential in the intermediate range is described by a finite power expansion with a nonlinear variable function ξ of internuclear separation R ,

$$\xi(R) = \frac{R - R_m}{R + bR_m}, \quad (1)$$

$$U_{\text{IR}}(R) = \sum_{i=0}^n a_i \xi(R)^i, \quad (2)$$

where $\{a_i\}$ are fitting parameters while b and R_m are chosen during the transform process from the spline representation to the analytic one, and R_m is close to the value of the equilibrium separation. The potential is continuously extrapolated for $R < R_i$ with

$$U_{\text{SR}}(R) = A + B/R^n \quad (3)$$

by adjusting the A and B parameters and n is fitted to find the best slope of the short range behavior.

For large internuclear distances ($R > R_o$) we adopted the standard long-range form of molecular potentials,

$$U_{\text{LR}}(R) = U_\infty - C_6/R^6 - C_8/R^8 - C_{10}/R^{10} \pm E_{\text{exch}}, \quad (4)$$

where the exchange contribution is given by

$$E_{\text{exch}} = A_{\text{ex}} R^\gamma \exp(-\beta R) \quad (5)$$

and U_∞ is the energy of the atomic asymptote (excluding the hyperfine energies) with respect to the minimum of the $X^1\Sigma^+$ state; $U_\infty - a_0$ coincides with the dissociation energy of the considered state, $D_e^{X/a}$. The exchange energy is repulsive for the triplet state [possessing plus sign in Eq. (4)] and attractive for the singlet state [minus sign in Eq. (4)]. All parameters in Eqs. (4) and (5) are common for $X^1\Sigma^+$ and $a^3\Sigma^+$ states.

The fit of the observations to this Hamiltonian is performed iteratively. First, we fit all rovibrational energies without hyperfine coupling but using the common asymptotic behavior of both states as given by Eq. (4). Second, we apply the hyperfine coupling in a coupled channel calculation to derive the energy corrections from the differences between the uncoupled solution and the coupled solution. We use those differences in the next potential fit to shift the original observations to the hypothetical energy levels of the uncoupled system. The new fit of the uncoupled case gives the improved potentials with which new corrections were calculated and the next iteration is started. The iteration procedure converges rapidly in few cycles. During this process the lines with strong deviations by hyperfine coupling (mainly $v''=23$ for $a^3\Sigma^+$ and $v''=94$ for $X^1\Sigma^+$) and those of $v''=29$ with doubtful assignment for the single-channel calculation could be incorporated. The $X^1\Sigma^+$ state levels with $v'' > 94$ for $X^1\Sigma^+$, which showed large deviations in the fit reported in [23] are described now satisfactorily in the present fit.

The overall fit quality can be demonstrated by the obtained normalized rms deviations: $\sigma=0.628$ for 14 320 transitions to the $X^1\Sigma^+$ state and $\sigma=0.864$ for 1937 transitions to the $a^3\Sigma^+$ state; these transitions are presented in the supplementary materials [30]. The derived parameters of the potential curves are given in Tables I and II for $X^1\Sigma^+$ and $a^3\Sigma^+$, respectively, as well as in supplementary materials [30]. To describe the long-range behavior we used for C_6 and C_8 the results from theoretical estimates by Derevianko *et al.* [33] and by Porsev and Derevianko [34]. The observed high v'' values allowed us to reach the long-range regime $R \geq 13$ Å since for $v''_a=29$ the outer turning point in the rotationless PEC is 14.8 Å while for $v''_X=97$ it is 12.7 Å. Since only few levels were measured there, the correlation would be strong within the full set of dispersion coefficients C_6 , C_8 , and C_{10} . Thus the best justified physical description will be obtained by fixing the theoretically well determined dispersion parameters and fitting the least accurately determined C_{10} .

In Fig. 6 significant deviations of the expected hyperfine structure are shown for some rotational levels N'' of the vibrational level $v''_a=23$. With the full modeling of both states these observations should become explainable. Coupled channel calculations were performed for these cases of N'' and it turned out that always the singlet level $v''_X=94$ is very close by, such that the hyperfine mixing is strong. The low frequency component in the five cases is an overlap of all singlet components and the $f=9/2$ manifold of the Cs hyperfine structure of the triplet [see for the coupling scheme at the end of Sec. III]. The middle component ($f=7/2$ from Cs)

TABLE II. Parameters of the analytic representation of the $a^3\Sigma^+$ state potential. The energy reference is the dissociation asymptote. Parameters with * are set for continuous extrapolation of the potential.

$R < R_i = 5.045$ Å	
A^*	-0.148797675×10^4 cm $^{-1}$
B^*	0.210042731×10^6 cm $^{-1}$ Å $^{3.06025}$
$R_i \leq R \leq R_o = 12.010$ Å	
b	-0.430
R_m	6.04984692 Å
a_0	-267.141122 cm $^{-1}$
a_1	$-0.134976112952988259 \times 10^1$ cm $^{-1}$
a_2	$0.151512740539140941 \times 10^4$ cm $^{-1}$
a_3	$-0.232360622185873837 \times 10^3$ cm $^{-1}$
a_4	$-0.174575068485499219 \times 10^4$ cm $^{-1}$
a_5	$-0.171945020361480820 \times 10^5$ cm $^{-1}$
a_6	$0.527754790994559880 \times 10^5$ cm $^{-1}$
a_7	$0.448967639930058038 \times 10^6$ cm $^{-1}$
a_8	$-0.207587042110053217 \times 10^7$ cm $^{-1}$
a_9	$-0.470797832797884103 \times 10^7$ cm $^{-1}$
a_{10}	$0.353746304452910498 \times 10^8$ cm $^{-1}$
a_{11}	$-0.146804315726933908 \times 10^7$ cm $^{-1}$
a_{12}	$-0.281279237533540189 \times 10^9$ cm $^{-1}$
a_{13}	$0.372686039456535578 \times 10^9$ cm $^{-1}$
a_{14}	$0.875871316553780675 \times 10^9$ cm $^{-1}$
a_{15}	$-0.239443645589827156 \times 10^{10}$ cm $^{-1}$
a_{16}	$0.382968717191889703 \times 10^9$ cm $^{-1}$
a_{17}	$0.426213900607794380 \times 10^{10}$ cm $^{-1}$
a_{18}	$-0.511104971641207314 \times 10^{10}$ cm $^{-1}$
a_{19}	$0.188097969655184364 \times 10^{10}$ cm $^{-1}$
$R > R_o$	
$D_{\text{asymptote}} = U_\infty$	0.0 cm $^{-1}$
C_6	0.2486300×10^8 cm $^{-1}$ Å 6
C_8	0.8934100×10^9 cm $^{-1}$ Å 8
C_{10}	0.3768824×10^{11} cm $^{-1}$ Å 10
A_{ex}	-0.3333495×10^6 cm $^{-1}$ Å $^{-\gamma}$
γ	4.88068
β	2.25698 Å $^{-1}$
Derived constants	
Equilibrium distance	$R_e^a = 6.05138(10)$ Å
Electronic term energy	$T_e^a = -267.141(20)$ cm $^{-1}$

is shifted strongly by the singlet mixing to the high frequency component ($f=5/2$ from Cs), which leads to an overlap of both for $N''=57$ and 59 . Because all components of the singlet manifold have also $f=7/2$ from Cs, the influence on the “middle” component of the unperturbed hyperfine structure of the triplet is strongest. In Fig. 6 results from these calculations are shown by short red sticks. The positions are well reproduced and would give the observed overlap of the

TABLE III. Predicted scattering lengths (in Bohr radius, $a_0 = 0.5292 \times 10^{-10}$ m). a_{lowest} gives the scattering length of the lowest hyperfine state.

Isotope	a_{singlet}	a_{triplet}	a_{lowest}	$K(f, m_f) + Cs(f, m_f)$
39/133	-15.3	84.8	71.7	(1, 1) + (3, 3)
40/133	-46.8	-32.8	-32.3	(9/2, -9/2) + (3, 3)
41/133	-66.7	216.4	196.3	(1, 1) + (3, 3)

manifold as seen in the recordings if we would have sufficient information of the relative intensities (also determined by the unknown singlet-triplet mixing in the excited state) for summing up all contributions with an appropriate line profile. But the goal of this work was to get the best modeling for the $X^1\Sigma^+ - a^3\Sigma^+$ system thus good energy description. This goal is well achieved as justified by Fig. 6 also.

V. MODELING COLD COLLISIONS

Up to now for the two-particle system K+Cs no cold collision studies are reported, but several laboratories are able to produce ultracold ensembles of either K or Cs atoms, and thus mixing both could be the next expected step. Therefore it is very interesting to predict such collision properties which might stimulate experimental studies on K+Cs. Table III gives the scattering lengths for s -wave scattering for the naturally appearing isotope combinations, calculated with the help of the present determined potentials for the singlet and triplet states of KCs. Additionally, Table III presents the predicted scattering lengths for the collisions of atomic pairs in their lowest hyperfine state.

Because we do not have data directly at the atom-pair asymptote, such as from Feshbach resonances or the last bound level, the potentials are extrapolated by the dispersion coefficients, where the lowest order C_6 is determined by theory with an accuracy of about 0.5%. This limits the accuracy of the predicted scattering lengths, but because all the values are not large in amplitude, we are quite certain that the sign of the scattering length is reliably determined. For the absolute values below $100a_0$ we estimate an error limit of about 20% and in the case of $^{41}\text{K } ^{133}\text{Cs}$ it is not larger than 50% for the triplet state and the hyperfine case.

Normally, the study of Feshbach resonances is of great help in understanding the collisional behavior of ultracold ensembles within magnetic fields. To show the richness of resonances in the case of K+Cs we calculated some of them in the field range up to 1000 G, which is typically obtainable in the experimental setups.

For the isotopolog $^{39}\text{K } ^{133}\text{Cs}$ four s -wave resonances are found for the lowest energy channel $f_K=1$, $m_f=1$ and $f_{Cs}=3$, $m_f=3$. Figure 8 shows the resonance profiles calculated for the scattering length to simplify experimental planning and considering how much the interaction can be tuned and how close other resonances are. The figure contains the resonance fields and the field strength of zero scattering length, from which the so-called width of the resonance can be derived. Around the resonance the calculations were performed

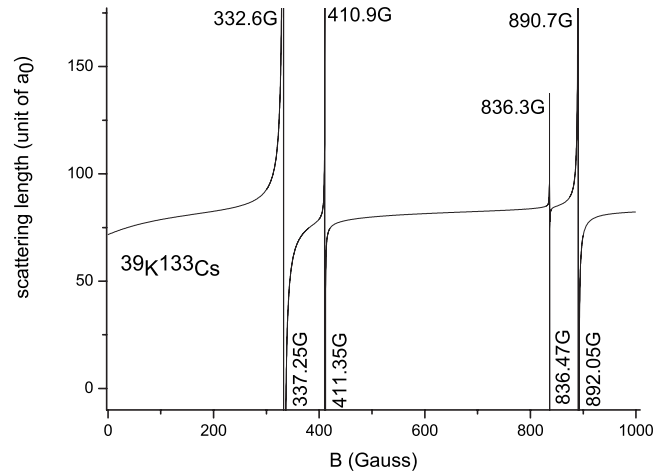


FIG. 8. Scattering length as a function of magnetic field for the collision channel $f_K=1$, $m_f=1$ and $f_{Cs}=3$, $m_f=3$ of $^{39}\text{K } ^{133}\text{Cs}$. The horizontally printed numbers are the positions of the resonances while the vertically printed ones denote the zero crossing of the scattering length. The number of digits shown is only needed to clearly identify the difference of the resonance position and the closest zero crossing of the scattering length, but it does not reflect the accuracy of the predictions of the position.

with 0.1 G digital resolution. The resonance at the low field of about 332 G with a width of 5 G could be very attractive for experimental studies. For the others at about 410, 836, and 890 G, the two lower ones are fairly sharp, but the highest has a width of about 1.5 G for easy access in experimental studies.

The structure for $^{41}\text{K } ^{133}\text{Cs}$ is even richer with six s -wave resonances for the entrance channel $f_K=1$, $m_f=1$ and $f_{Cs}=3$, $m_f=3$, where the high field resonance around 867 G has a width of about 5 G, the others are sharper. For the isotopolog $^{40}\text{K } ^{133}\text{Cs}$ we get for the entrance channel $f_K=9/2$, $m_f=-9/2$ and $f_{Cs}=3$, $m_f=3$ two very narrow s -wave resonances at 254 and 449 G, their width is below 0.1 G. From calculations on the Zeeman structure of the bound levels at the atomic asymptote 13 more resonances are expected for fields up to 1000 G, but they are so sharp that digital resolutions in the calculations better than 1 mG are needed for identification. All predictions of the s -wave resonances use extrapolations of the potential curves, thus error estimates are difficult. We believe that the low field positions should be good to 50 G.

VI. CONCLUSION

With new and very much extended spectroscopic data for $^{39}\text{K } ^{133}\text{Cs}$ compared to Ref. [23], especially on the triplet state $a^3\Sigma^+$, we derived potential energy curves which describe all experimental data (in total 15 655 transitions, including earlier published values for the singlet state from [23]) within experimental error limits, most of them at 0.003 cm^{-1} . From a large set of data for pairs of transitions with a common upper level, the energy separation between the manifold of rovibrational levels of the singlet and the triplet states is reliably determined where both potential

curves are coupled by the same long-range behavior. The dissociation energies (with respect to the center of gravity of HFS asymptote) are $D_e^X=4069.208(40)$ cm $^{-1}$ and $D_e^a=267.141(20)$ cm $^{-1}$. The potentials will serve for predicting all bound states of the X $^1\Sigma^+$ - $a^3\Sigma^+$ coupled system and thus will help in analyzing the rovibrational structure of the excited states from optical spectra by applying selection rules and Franck-Condon principle. This can accelerate further studies on KCs with goals such as producing ultracold KCs molecules.

We presented some collision properties for cold collision of K+C_s, which we believe are valuable in preparing respective experiments. With the respective data it would be straightforward to perform similar calculations for other entrance channels of the atomic collision process. If experimental Feshbach resonances on KCs become available, our

results would be the starting point for obtaining improved potentials in the long-range regime.

ACKNOWLEDGMENTS

We are grateful to Dr. Andrei Jarmola for providing the laser diodes built in homemade external cavity resonators. The support from the Latvian Science Council Grant No. 09.1036 is gratefully acknowledged by Riga team. The team at Hannover acknowledges the support by the DFG through Grant No. SFB 407 and the newly founded center of excellence QUEST "Quantum Engineering and Space-Time Research." A.P. acknowledges partial support from the Bulgarian National Science Fund Grants No. VUF 202/06 and No. VUI 301/07.

-
- [1] R. V. Krems, *Int. Rev. Phys. Chem.* **24**, 99 (2005).
 - [2] P. Rabl, D. DeMille, J. M. Doyle, M. D. Lukin, R. J. Schoelkopf, and P. Zoller, *Phys. Rev. Lett.* **97**, 033003 (2006).
 - [3] T. Zelevinsky, S. Kotochigova, and Jun Ye, *Phys. Rev. Lett.* **100**, 043201 (2008).
 - [4] D. DeMille, S. Sainis, J. Sage, T. Bergeman, S. Kotochigova, and E. Tiesinga, *Phys. Rev. Lett.* **100**, 043202 (2008).
 - [5] V. V. Flambaum and M. G. Kozlov, *Phys. Rev. Lett.* **99**, 150801 (2007).
 - [6] T. V. Tscherbul and R. V. Krems, *Phys. Rev. Lett.* **97**, 083201 (2006).
 - [7] K.-K. Ni, S. Ospelkaus, M. H. G. de Miranda, A. Pe'er, B. Neyenhuys, J. J. Zirbel, S. Kotochigova, P. S. Julienne, D. S. Jin, and J. Ye, *Science* **322**, 231 (2008).
 - [8] D. Wang, J. T. Kim, C. Ashbaugh, E. E. Eyler, P. L. Gould, and W. C. Stwalley, *Phys. Rev. A* **75**, 032511 (2007).
 - [9] F. Ferlaino, C. D'Errico, G. Roati, M. Zaccanti, M. Inguscio, G. Modugno, and A. Simoni, *Phys. Rev. A* **73**, 040702(R) (2006).
 - [10] F. Ferlaino, C. D'Errico, G. Roati, M. Zaccanti, M. Inguscio, G. Modugno, and A. Simoni, *Phys. Rev. A* **74**, 039903(E) (2006).
 - [11] S. Ospelkaus, C. Ospelkaus, L. Humbert, K. Sengstock, and K. Bongs, *Phys. Rev. Lett.* **97**, 120403 (2006).
 - [12] S. D. Kraft, P. Staunum, J. Lange, L. Vogel, R. Wester, and M. Weidemüller, *J. Phys. B* **39**, S993 (2006).
 - [13] J. Deiglmayr, A. Grochola, M. Repp, K. Mörtlbauer, C. Glück, J. Lange, O. Dulieu, R. Wester, and M. Weidemüller, *Phys. Rev. Lett.* **101**, 133004 (2008).
 - [14] J. P. Shaffer, W. Chalupczak, and N. P. Bigelow, *Phys. Rev. Lett.* **82**, 1124 (1999).
 - [15] C. Haimberger, J. Kleinert, M. Bhattacharya, and N. P. Bigelow, *Phys. Rev. A* **70**, 021402(R) (2004).
 - [16] J. M. Sage, S. Sainis, T. Bergeman, and D. DeMille, *Phys. Rev. Lett.* **94**, 203001 (2005).
 - [17] A. J. Kerman, J. M. Sage, S. Sainis, T. Bergeman, and D. DeMille, *Phys. Rev. Lett.* **92**, 153001 (2004).
 - [18] A. Pashov, O. Docenko, M. Tamanis, R. Ferber, H. Knöckel, and E. Tiemann, *Phys. Rev. A* **72**, 062505 (2005).
 - [19] O. Docenko, M. Tamanis, J. Zaharova, R. Ferber, A. Pashov, H. Knöckel, and E. Tiemann, *J. Phys. B* **39**, S929 (2006).
 - [20] P. Staunum, A. Pashov, H. Knöckel, and E. Tiemann, *Phys. Rev. A* **75**, 042513 (2007).
 - [21] A. Pashov, O. Docenko, M. Tamanis, R. Ferber, H. Knöckel, and E. Tiemann, *Phys. Rev. A* **76**, 022511 (2007).
 - [22] M. Aymar and O. Dulieu, *J. Chem. Phys.* **122**, 204302 (2005).
 - [23] R. Ferber, I. Klincare, O. Nikolayeva, M. Tamanis, H. Knöckel, E. Tiemann, and A. Pashov, *J. Chem. Phys.* **128**, 244316 (2008).
 - [24] M. Korek, A. R. Allouche, K. Fakhreddine, and A. Chaalan, *Can. J. Phys.* **78**, 977 (2000).
 - [25] M. Korek, Y. A. Moghrabi, and A. R. Allouche, *J. Chem. Phys.* **124**, 094309 (2006).
 - [26] M. Aymar and O. Dulieu (private communication).
 - [27] A. Pashov, P. Popov, H. Knöckel, and E. Tiemann, *Eur. Phys. J. D* **46**, 241 (2008).
 - [28] F. Xie, V. B. Sovkov, A. M. Lyyra, D. Li, S. Ingram, J. Bai, V. S. Ivanov, S. Magnier, and Li Li, *J. Chem. Phys.* **130**, 051102 (2009).
 - [29] A. Pashov, W. Jastrzębski, and P. Kowalczyk, *Comput. Phys. Commun.* **128**, 622 (2000).
 - [30] See EPAPS Document No. E-PLRAAN-80-128911 for point-wise $a^3\Sigma^+$ state PEC, for LIF transitions frequencies used to fit potentials, and for parameters of analytic representation of X $^1\Sigma^+$ PEC and of $a^3\Sigma^+$ PEC. For more information on EPAPS, see <http://www.aip.org/pubservs/epaps.html>.
 - [31] S. Falke, H. Knöckel, J. Friebe, M. Riedmann, E. Tiemann, and C. Lisdat, *Phys. Rev. A* **78**, 012503 (2008).
 - [32] E. Arimondo, M. Inguscio, and P. Violino, *Rev. Mod. Phys.* **49**, 31 (1977).
 - [33] A. Derevianko, J. F. Babb, and A. Dalgarno, *Phys. Rev. A* **63**, 052704 (2001).
 - [34] S. G. Porsev and A. Derevianko, *J. Chem. Phys.* **119**, 844 (2003).